Int. J. Electrochem. Sci., 17 **(2022)** Article Number: 220731, doi: 10.20964/2022.07.11

International Journal of
ELECTROCHEMICAL
SCIENCE
www.electrochemsci.org

A Powerful Electrochemical Sensor Based on Fe_2O_3 nanoparticle-Graphene Oxide Nanocomposites for Determination of Metronidazole as an Antibacterial Drug

Ziping Liu, Zhangjie Wang[*]*, Yan Xu*

College of Pharmacy, Anhui Xinhua University, Hefei, 230088 , China
[*]E-mail: lzp501526848@sina.com

Received: 8 March 2022 / *Accepted:* 21 April 2022 / *Published:* 6 June 2022

This research focused on the hydrothermal synthesis of Fe_2O_3 nanoparticle-Graphene oxide nanocomposites modified glassy carbon electrode (Fe_2O_3@GO/GCE) as an electrochemical sensor for determining the antibacterial medication Metronidazole (MNZ). Fe_2O_3@GO nanocomposite production was confirmed by SEM and XRD studies. Electrochemical studies using DPV and amperometry techniques revealed that Fe_2O_3@GO/GCE as a sensitive and selective MNZ sensor had comparable and even better sensing performance than previously reported MNZ sensors, which was attributed to Fe_2O_3@GO nanocomposite's synergistic electrocatalytic effects for MNZ electrochemical sensing. The liner range, the sensitivity and the detection limit were estimated at 1 to 1680µM, 0.02289µA/µM and 55nM, respectively. The validity and precision of the proposed amperometry sensing method for determining MNZ were evaluated in five different urine samples from patients aged 45-60 years old who were given MNZ, and the findings of the amperomery and ELISA assays were found to be in good agreement, implying that the proposed system had high detection accuracy and validity for determining MNZ in clinical samples.

Keywords: Electrochemical sensor; Metronidazole; Antibacterial drug; Fe_2O_3 nanoparticle; graphene oxide

1. INTRODUCTION

Metronidazol (MNZ; 2-(2-methyl-5-nitroimidazol-1-yl)ethanol) is an imidazole-class synthetic antibacterial and antiprotozoal drug with 2-hydroxyethyl, nitro, and methyl groups substituted at C-1, -2, and -5, respectively [1-3]. MNZ enters the body and suppresses protein production by interacting with DNA, causing strand breakage and loss of helical DNA structure [4, 5].

As a result, it causes cell death in sensitive organisms and is very active against both gram-negative and gram-positive anaerobic bacteria, such as B. fragilis and C. difficile [6-8]. MNZ is

therefore used to treat bacterial infections of the vaginal canal, stomach, liver, skin, joints, brain, spinal cord, lungs, heart, and circulation [9-11]. On the other hand, MNZ may cause nausea, diarrhea, constipation, upset stomach, stomach cramps, loss of appetite, and headaches [12-14]. As a result, identifying and detecting MNZ levels in clinical samples is critical, particularly for patients on high-dose antibiotic medication [15-17].

Several analytical methods have been investigated for the identification and determination of MNZ levels in biological fluids and clinical samples, which include high performance liquid chromatography [18, 19], spectrophotometry [20], fluorometry [21], gas chromatography [22], surface enhanced Raman spectroscopy [23], polarography [24], and electrochemical methods [25-38]. Between the above analytical methods, electrochemical methods have been showed to have good selectivity and a broad linear range toward MNZ determination in clinical samples [39-41]. However, many studies have been conducted on improve the stability, sensitivity and detection limit of MNZ electrochemical sensors using nanostructures and various hybrids and nanocomposites [42, 43]. To the best of our knowledge, many of these studies showed the limited linear range which limits the application of these electrochemical sensors for the determination of MNZ level in pharmaceutical samples [25-32]. As a result, the focus of this research has been on the fabrication of Fe_2O_3@GO nanocomposites as a stable and wide range electrochemical sensor for determining the antibacterial medication Metronidazole.

2. EXPERIMENTAL SECTION

2.1. Preparation of Fe_2O_3@GO nanocomposites

A hydrothermal method was applied for preparation of Fe_2O_3@GO nanocomposites [44]: 1.5 g of $NaCH_3COO$ (≥99.0%, Luoyang Tongrun Info Technology Co., Ltd., China) and 0.6 g of $FeCl_3 \cdot 6H_2O$ (≥99%, Evergreen Chemical Factory Co., Ltd., China) were ultrasonically mixed with 22 mL ethanol (99.9%, Evergreen Chemical Factory Co., Ltd., China) and 8 mL of deionized water. After sonication for 40 minutes, the mixture was transferred to a 100 ml Teflon-lined stainless steel autoclave, and the autoclave was heated at 190°C for 10 hours. After cooling, the precipitates were collected and washed with ethanol several times, and dried in an oven at 75 °C for 5 hours. The resulted Fe_2O_3 NPs were utilized for the preparation of Fe_2O_3@GO nanocomposites in the following steps: 0.05 g of GO (99%, Luoyang Tongrun Info Technology Co., Ltd., China) and 0.5 g Fe_2O_3 NPs were ultrasonically added into 10 mL of deionized water for 20 minutes at room temperature to achieve a uniform suspension. Then, the suspension was transferred to a 50 ml Teflon-lined stainless steel autoclave, and the autoclave was heated at 100°C for 5 hours. Finally, the obtained Fe_2O_3@GO nanocomposite was collected and washed with ethanol several times. For modification of the GCE surface with Fe_2O_3@GO nanocomposite, 2 mg of Fe_2O_3@GO was ultrasonically dispersed in 2 mL of a mixture of ethanol and nafion (20 wt.%, Sigma-Aldrich) solution for 25 minutes, and 50 μL of the obtained homogeneous black suspension was dropped onto the clean surface of GCE and dried at room temperature.

2.2. Analysis of real sample

The amount of MNZ in human urine samples from patients receiving MNZ medication was determined using an amperometric approach. All urine samples were centrifuged at 1000 rpm for 10 minutes prior to analysis, and the supernatant was used to prepare 0.1M PBS with a pH of 7.0 without any purification. The RSD values were calculated using the standard addition method. For determining the MNZ content in patients' urine samples, the MNZ ELISA Kits (E4948-100, Absorbance: 450 nm, BioVision, USA) were also used.

2.3. Structural and electrochemical characterizations

Crystallographic and morphological characterizations were performed using an X-ray difractometer (XRD; D8 Advance, with Cu Kα (λ=1.5405Å), Germany) and scanning electron microscopy (SEM; JSM-5600LV, JEOL, Tokyo, Japan), respectively. Electrochemical characterizations were conducted on amperometry and differentialpulse voltammetry (DPV) techniques by potentiostat-galvanostat in a three-electrode configuration consisted of modified GCE, Pt plate, and Ag/AgCl as a working, counter and reference electrodes, respectively, in 0.1 M phosphate buffer solution (PBS) with pH 7.0 which prepared by mixing stock solutions of by 0.1 M NaCl (99%, Sigma-Aldrich),and 0.1 M NaH_2PO_4–Na_2HPO_4 (99%, Sigma-Aldrich). Adjusting the solution's pH was performed with 0.1 M NaOH (99%, Sigma-Aldrich) or 0.01 M H_3PO_4 (99%, Sigma-Aldrich). All solutions were prepared at room temperature, and all measurements were carried out at room temperature.

3. RESULTS AND DISCUSSION

3.1. Structural characterizations

SEM images of pure GO nanosheets and Fe_2O_3@GO nanocomposite modified GCE are shown in Figures 1a and 1b, respectively. Individual nanosheets are intimately connected in the SEM pictures of GO nanosheets, which display the wavy and folded form of GO thin layers in addition to the wavy and folded shape of GO thin layers. The Fe_2O_3@GO nanocomposite SEM pictures demonstrate that Fe_2O_3 NPs of various sizes and shapes are randomly implanted into the GO nanosheets in the nanocomposite. Fe_2O_3 NPs have an average diameter of 72 nm.

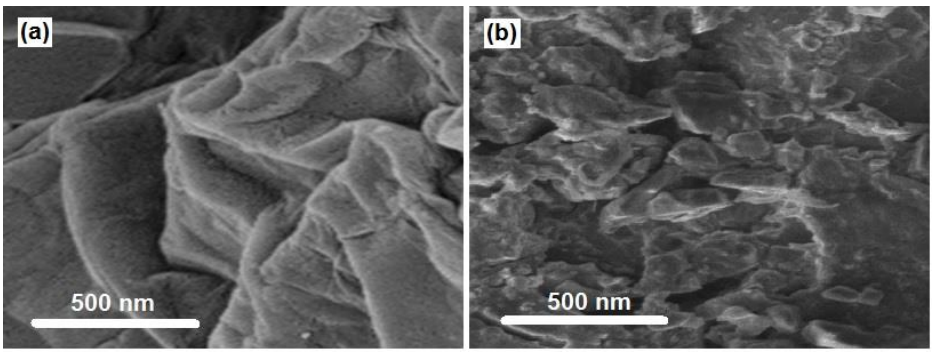

Figure 1. SEM micrographs of (a) pure GO nanosheets and (b) Fe_2O_3@GO nanocomposite modified GCE.

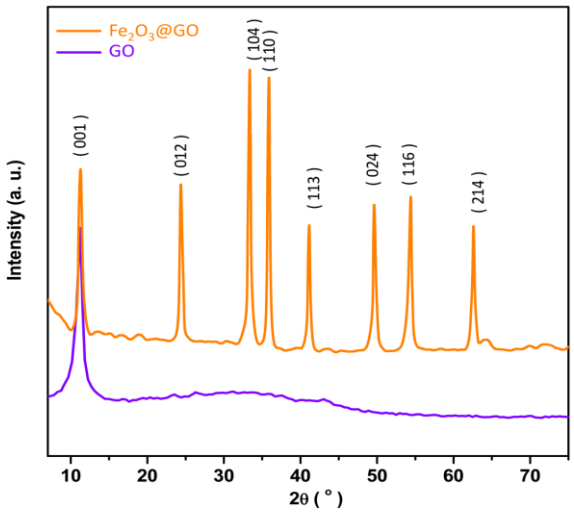

Figure 2. XRD patterns of pure GO nanosheets and Fe_2O_3@GO nanocomposite.

Figures 2a and 2b depict the XRD patterns of pure GO nanosheets and Fe_2O_3@GO nanocomposite, respectively. As seen, the XRD pattern of GO nanosheets exhibits a single strong diffraction peak at 11.17° which is assigned to the diffraction graphitic plane of (001) of GO [45-47]. XRD pattern of Fe_2O_3@GO shows diffraction peaks at 24.32°, 33.18°, 35.74°, 41.03°, 49.61, 54.32 and 62.61° are corresponding to (012), (104), (110), (113) , (024), (116) and (214) planes of hematite of α-Fe_2O_3 (JCPDS card no. 04-015-9569) [48-50], respectively, and additional diffraction peak of (001) of GO. Therefore, the results of crystallographic and morphological characterizations confirm the successful formation of Fe_2O_3@GO nanocomposite.

3.2. Electrochemical characterizations

Electrochemical responses of unmodified and modified GCE in the absence and presence of 100 µM MNZ in 0.1 M PBS with pH 7.0 at a scan rate of 50mV/s are depicted in Figure 3. As seen in

the absence of MNZ solution in the electrochemical cell, DPV plots of GCE, GO/GCE and Fe_2O_3@GO/GCE do not display any clear redox peak. However, there was a cathodic peak for all electrodes after the addition of MNZ solution which corresponded to catalytically reduction of the nitro group of MNZ [51-53]. The mechanism of a possible electro-reduction of MNZ is described in Figure 4 [54, 55]. The reduction peak is observed at a potential of -0.50 V, -0.47 V and -0.45 V for GCE, GO/GCE and Fe_2O_3@GO/GCE, respectively. Moreover, the peak current for reduction of MNZ obtained by Fe_2O_3@GO/GCE is approximately 3-fold and 2-fold higher than GCE and GO/GCE, respectively. It demonstrates that the Fe_2O_3@GO nanocomposite shows significant catalytic attractive in the reductive reaction of MNZ because of presence of Fe_2O_3 NPs with intrinsic enzyme-mimicking activity and non-toxicity which exhibit remarkable catalytic properties in electrochemical reactions because of their great oxygen ion mobility at the electrode surface [56-58]. Furthermore, as lightweight absorbers, GO nanosheets have a large effective surface area, structural defects sites, and surface oxygen functional groups on their surface, as well as high porosity and significant electrical conductivity [59-61]. Thus, in Fe_2O_3@GO nanocomposite, Fe_2O_3 NPs and GO nanosheets can form appropriate electron pathways between the electrolyte and the electrode surface [62-64]. In addition, embedding Fe_2O_3 NPs into the GO nanosheets restricts the GO nanosheets aggregation and enhances the effective surface area of the nanocomposite than that of GO nanosheet alone, and according to SEM results, embedded Fe_2O_3 NPs are electrochemically accessible and highly active [60, 65, 66]. Therefore, the Fe_2O_3@GO/GCE shows the higher peak current and lower reduction potential of MNZ. Cathodic peak potential shifted to a lower potential value confirming the irreversibility of the reduction reaction of MTZ at Fe_2O_3@GO [67]. As a result of the above DPV measurements, it was determined that Fe_2O_3@GO/GCE has higher catalytic activity toward MNZ sensing than GCE and GO/GCE, and was chosen as a favorable catalyst for subsequent electrochemical studies of MNZ sensing.

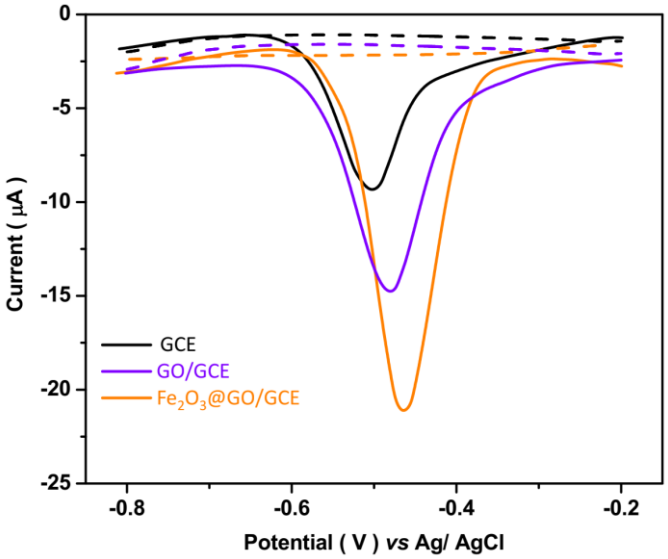

Figure 3. DPV plots of GCE, GO/GCE and Fe_2O_3@GO/GCE in absence (dashed line) and presence (solid line) of 100 µM MNZ in 0.1 M PBS with pH 7.0 at a scan rate of 50 mV/s.

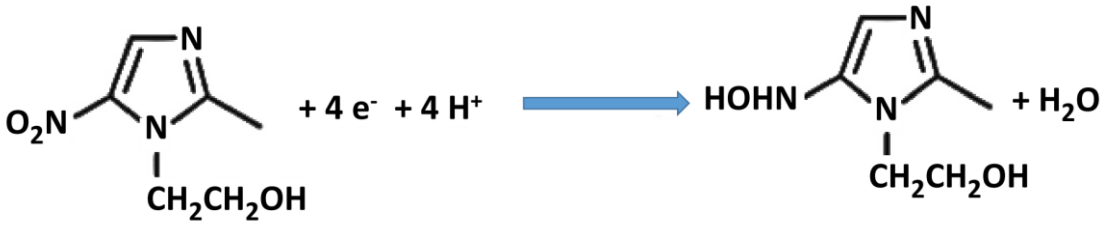

Figure 4. The proposed mechanism of MNZ electro-reduction

Figure 5a illustrates the amperometric response of Fe_2O_3@GO/GCE to consecutive additions of 60 µM MNZ at a potential of -0.45 V in 0.1 M PBS with pH 7.0. As observed, the Fe_2O_3@GO/GCE exhibits a relatively fast response to any addition of MNZ solution, indicating rapid electron transfer on the Fe_2O_3@GO/GCE surface associated with easy desorption of reaction intermediates and easy diffusion of analyte molecules [68-70]. Figure 5b shows the related calibration graph which indicates the linear increase of electrocatalytic current with consecutive additions of 60 µM MNZ from 1 to 1680 µM. Additionally, the sensitivity and detection limit (S/N=3) are estimated at 0.02289 µA/µM and 55 nM, respectively. The results are compared with other MNZ electrochemical sensors reported in the literature (Table 1).

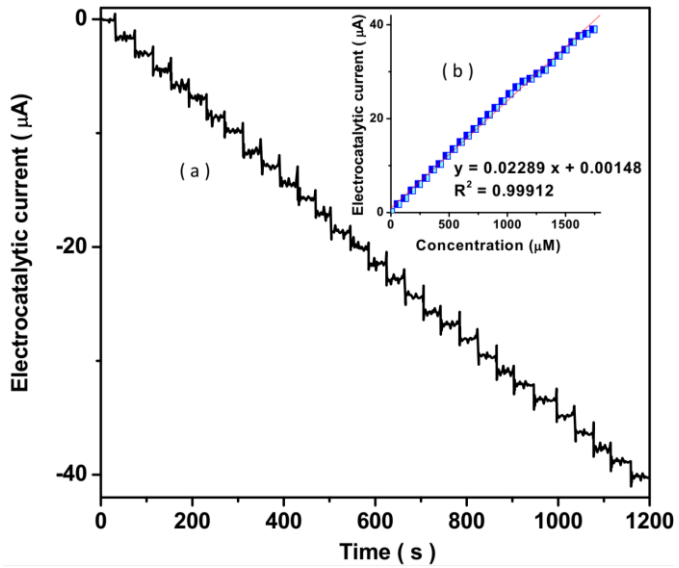

Figure 5. (a) Amperometric of Fe_2O_3@GO/GCE to consecutive additions of 60 µM MNZ at potential of -0.45 V in 0.1 M PBS with pH 7.0; (b) The related calibration graph

As found, Fe_2O_3@GO/GCE shows the comparable and even better sensing performance than the other sensors which is attributed to the synergistic electrocatalytic effects of Fe_2O_3@GO nanocomposite for the electrochemical sensing of MNZ. Fe_2O_3 nanoparticles increase the effective

surface area of the electrolyte and reversible redox reaction [71-73]. GO nanosheets also serve as an efficient electron shuttling mediator–enhancing the sensor performance [60, 74].

The effect of various substances in pharmaceuticals and/or in biological fluids as compounds potentially interfering with the detection of MNZ was evaluated using amperometric measurements of Fe_2O_3@GO/GCE under consecutive additions of MNZ and 5-fold of interfering substances at a potential of -0.45 V in 0.1 M PBS with pH 7.0. Table 2 presents the results of amperometric signals at a potential of -0.45 V that indicated a remarkable amperometric response to the addition of MNZ in the electrochemical cell, and insufficient signal to consecutive additions of interfering substances. As a result, there is no discernible interference effect for MNZ determination in the presence of various pharmaceutical compounds, and the developed Fe_2O_3@GO/GCE has high selectivity for MNZ determination.

Table 1. Comparison of analytical sensing performance for determination of MNZ over various modified electrodes.

Electrodes	Technique	Detection limit (nM)	Linear range (µM)	Ref.
Fe_2O_3@GO/GCE	Amperometry	35	1 to 1680	This study
Graphene nanoflakes/GCE	Amperometry	0.15	0.0005 to 0.0055	[37]
MWCNTs/chitosan-nickel complex/GCE	DPV	25	0.1 to 150	[29]
Molecularly imprinted polymer/ graphene quantum dots/graphene nanoplatelets/GCE	DPV	0.52	0.75 to 10.0	[28]
$CuCo_2O_4$/N-CNTs/GCE	DPV	0.48	0.1 to 100	[27]
N, S, P-triple doped porous carbon	LSV	13	50 to 350	[26]
Carbon nanofibers@Au NPs	DPV	24	0.1 to 2000	[36]
Cysteic acid and poly(diallydimethylammonium chloride)-functionalized graphene/GCE	DPV	2.3	70 to 800	[35]
Oxygen-doped graphitic carbon nitride /GCE	DPV	5	0.01 to 2060	[34]
Fe-doped metal-organic framework/GCE	LSV	165	0.5 to 30	[25]
Molecularly imprinted polymer/AuNPs/GCE	DPV	120	0.5 to 1000	[33]
SrV_2O_6/GCE	CV	4	0.01 to 207	[32]
Activated screen printed carbon electrode	DPV	10	0.05 to 563	[31]
Magnetic molecularly imprinted polymer/GCE	DPV	16	0.05 to 1.0	[30]
Ag/Au/Nafion/GCE	DPV	58.7	100 to 1000	[38]

LSV: linear sweep voltammetry, CV: Cyclic voltammetry

The validity and precision of the proposed amperometry sensing method was evaluated for the determination of MNZ in five different urine samples from patients aged 45-60 years old who were administrated MNZ. Figure 6 shows the amperomeric response and related calibration graph of Fe_2O_3@GO/GCE tossive adding of MNZ solution in prepared 0.1 M PBS with pH 7.0 of human urine samples at -0.45 V. It demonstrates that the MNZ concentration in the prepared sample of urine of first patient (S1) is 0.069 µM, it is worth noting that the viability value obtained by the amperometric assay is similar to that obtained by the MNZ ELISA kit assay (Table 3). These assays were also carried out for the other four samples and findings of an average of 4 times of amperomery and ELISA assays to

determination of MNZ are exhibited in Table 3. As may be shown, amperomery and ELISA assays have a high level of agreement [75, 76]. Moreover, Table 3 shows that the obtained RSD values are less than 4.41%, respectively, implying that the proposed system has a great detection accuracy, and validity for the determination of MNZ in clinical samples.

Table 2. Results of study of interfering effect of various substances with the detection of MNZ using amperometric measurements of Fe_2O_3@GO/GCE under consecutive additions of MNZ and 5-fold of interfering substances at potential of 0.55 V in 0.1 M PBS with pH 7.0.

Substance	**Added (µM)**	**Amperometric current (µA) at -0.45 V**	**RSD (%)**
MNZ	10	0.2292	±0.0077
Caffeine	50	0.0164	±0.0017
Cystine	50	0.0123	±0.0018
Cellulose	50	0.0220	±0.0010
Glucose	50	0.0211	±0.0011
Chloramphenicol	50	0.0305	±0.0015
Dopamine	50	0.0221	±0.0009
Nitrophenol	50	0.0431	±0.0010
Ascorbic Acid	50	0.0222	±0.0012
Thiamphenicol	50	0.0580	±0.0015
Oxalic Acid	50	0.0204	±0.0023
4-Nitrobenzoic Acid	50	0.0110	±0.0015
Uric Acid	50	0.0105	±0.0010
Orinidazole	50	0.0251	±0.0018
4-Nitroaniline	50	0.0253	±0.0011
Florfenicol	50	0.0340	±0.0019
4-nitrophenol	50	0.0104	±0.0009
KCl	50	0.0092	±0.0007
$NaNO_3$	50	0.0109	±0.0008
$CaCl_2$	50	0.0088	±0.0005
$MgSO_4$	50	0.0072	±0.0009

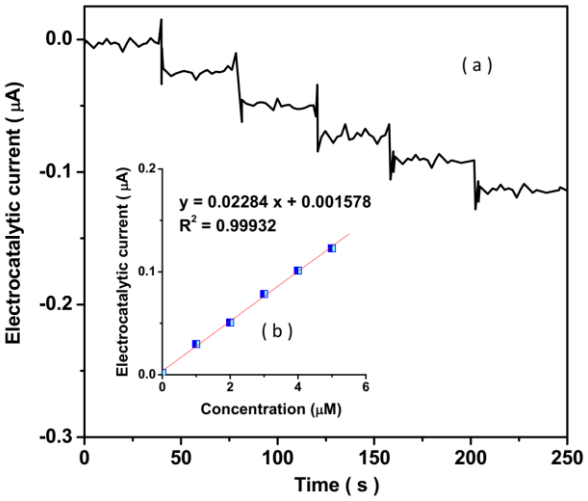

Figure 6. (a) Amperomeric response and (b) related calibration graph of Fe_2O_3@GO/GCE tosuccessive adding MNZ solution in prepared 0.1 M PBS with pH 7.0 of human urine samples at -0.45 V.

Table 3. The results of determination of MNZ in five different in urine samples from patients aged 45-60 years old who administrated MNZ using the ELISA and amperometry assays.

Sample	**Concentration of** MNZ **in prepared urine samples (µM)**			
	Amperometry		MNZ **ELISA kit**	
	Fe_2O_3@GO/GCE	**RSD (%)**	**ELISA**	**RSD (%)**
S1	0.069	±3.75	0.067	±3.20
S2	0.051	±3.88	0.055	±4.39
S3	0.049	±4.41	0.046	±4.40
S4	0.066	±3.10	0.070	±3.03
S5	0.058	±3.41	0.053	±3.26

4. CONCLUSION

This study focused on the synthesis of Fe_2O_3@GO/GCE as the electrochemical sensor for the determination of Metronidazole as an antibacterial drug. A hydrothermal method was applied for preparation of nanocomposites. SEM and XRD analyses confirmed the successful formation of the Fe_2O_3@GO nanocomposite. Electrochemical studies showed that Fe_2O_3@GO/GCE as the sensitive and selective MNZ sensor indicated comparable and even better sensing performance than the other reported MNZ sensors. The liner range, the sensitivity and the detection limit were estimated at 1 to 1680 µM, 0.02289 µA/µM and 55 nM, respectively. The validity and precision of the proposed amperometry sensing method were evaluated for the determination of MNZ in five different urine samples from patients aged 45-60 years old who were administrated MNZ. The findings of the amperomery and ELISA assays were found to be in good agreement, implying the proposed system had great detection accuracy, and validity for the determination of MNZ in clinical samples.

ACKNOWLEDGEMENT
This work was sponsored in part by Natural Science Project of Anhui Provincial Department of Education (KJ2020A0790), University Key Scientific Research Project (2019zr004).

References

1. X. Wang, A. Wang, M. Lu and J. Ma, *Chemical engineering journal*, 337 (2018) 372.
2. B. Zhou, Z. Liu, C. Li, M. Liu, L. Jiang, Y. Zhou, F.L. Zhou, S. Chen, S. Jerrams and J. Yu, *Advanced electronic materials*, 7 (2021) 2100233.
3. K.A. Zahidah, S. Kakooei, M. Kermanioryani, H. Mohebbi, M.C. Ismail and P.B. Raja, *International Journal of Engineering and Technology Innovation*, 7 (2017) 243.
4. X. Tang, J. Wu, W. Wu, Z. Zhang, W. Zhang, Q. Zhang, W. Zhang, X. Chen and P. Li, *Analytical chemistry*, 92 (2020) 3563.
5. M. Yang, C. Li, Y. Zhang, D. Jia, R. Li, Y. Hou, H. Cao and J. Wang, *Ceramics International*, 45 (2019) 14908.
6. C. Alauzet, A. Lozniewski and H. Marchandin, *Anaerobe*, 55 (2019) 40.
7. X. Hu, P. Zhang, D. Wang, J. Jiang, X. Chen, Y. Liu, Z. Zhang, B.Z. Tang and P. Li, *Biosensors and Bioelectronics*, 182 (2021) 113188.

8. J. Rouhi, S. Mahmud, S. Hutagalung and S. Kakooei, *Micro & Nano Letters*, 7 (2012) 325.
9. B. Bai, Q. Nie, H. Wu and J. Hou, *Powder Technology*, 394 (2021) 1158.
10. T. Gao, C. Li, Y. Zhang, M. Yang, D. Jia, T. Jin, Y. Hou and R. Li, *Tribology International*, 131 (2019) 51.
11. R. Mohamed, J. Rouhi, M.F. Malek and A.S. Ismail, *International Journal of Electrochemical Science*, 11 (2016) 2197.
12. R.I. Almeida-Secaira, O.P. Núñez-Torres, P.A. Paredes-Carvajal and C.A. Cuadrado-Guevara, *Journal of the Selva Andina Animal Science*, 6 (2019) 3.
13. S. Guo, C. Li, Y. Zhang, Y. Wang, B. Li, M. Yang, X. Zhang and G. Liu, *Journal of Cleaner Production*, 140 (2017) 1060.
14. F. Jin, Z.-S. Qian, Y.-M. Chu and M. ur Rahman, *Journal of Applied Analysis & Computation*, 12 (2022) 790.
15. W.-F. Lai and W.-T. Wong, *Asian Journal of Pharmaceutical Sciences*, 16 (2021) 577.
16. J. Zhang, C. Li, Y. Zhang, M. Yang, D. Jia, G. Liu, Y. Hou, R. Li, N. Zhang and Q. Wu, *Journal of cleaner production*, 193 (2018) 236.
17. K. Eswar, J. Rouhi, H. Husairi, M. Rusop and S. Abdullah, *Advances in Materials Science and Engineering*, 2014 (2014) 1.
18. C. Akay, S.A. Özkan, Z. Şentürk and Ş. Cevheroğlu, *Il Farmaco*, 57 (2002) 953.
19. T.-H. Zhao, M.-K. Wang, W. Zhang and Y.-M. Chu, *Journal of Inequalities and Applications*, 2018 (2018) 1.
20. P. Nagaraja, K. Sunitha, R. Vasantha and H. Yathirajan, *Journal of Pharmaceutical and Biomedical Analysis*, 28 (2002) 527.
21. S. Yang, L. Wang, L. Zuo, C. Zhao, H. Li and L. Ding, *Microchimica Acta*, 186 (2019) 1.
22. C. Ho, D.W. Sin, K. Wong and H.P. Tang, *Analytica chimica acta*, 530 (2005) 23.
23. C. Han, J. Chen, X. Wu, Y.-w. Huang and Y. Zhao, *Talanta*, 128 (2014) 293.
24. G. El-Sayed, *Microchemical journal*, 55 (1997) 110.
25. Y. Baikeli, X. Mamat, F. He, X. Xin, Y. Li, H.A. Aisa and G. Hu, *Ecotoxicology and Environmental Safety*, 204 (2020) 111066.
26. N. Yalikun, X. Mamat, Y. Li, X. Hu, P. Wang and G. Hu, *Journal of The Electrochemical Society*, 166 (2019) B1131.
27. Y. Wang, L. Yao, X. Liu, J. Cheng, W. Liu, T. Liu, M. Sun, L. Zhao, F. Ding, Z. Lu, P. Zou, X. Wang, Q. Zhao and H. Rao, *Biosensors and Bioelectronics*, 142 (2019) 111483.
28. A.A. Ensafi, P. Nasr-Esfahani and B. Rezaei, *Sensors and Actuators B: Chemical*, 270 (2018) 192.
29. A. Mao, H. Li, L. Yu and X. Hu, *Journal of Electroanalytical Chemistry*, 799 (2017) 257.
30. D. Chen, J. Deng, J. Liang, J. Xie, C. Hu and K. Huang, *Sensors and Actuators B: Chemical*, 183 (2013) 594.
31. P. Sundaresan, T.-W. Chen, S.-M. Chen, T.-W. Tseng and X. Liu, *International Journal of Electrochemical Science*, 13 (2018) 1441.
32. R. Karthik, J.V. Kumar, S.-M. Chen, P.S. Kumar, V. Selvam and V. Muthuraj, *Scientific Reports*, 7 (2017) 7254.
33. Y. Gu, X. Yan, C. Li, B. Zheng, Y. Li, W. Liu, Z. Zhang and M. Yang, *Biosensors and Bioelectronics*, 77 (2016) 393.
34. G. Kesavan, V. Vinothkumar, S.-M. Chen and T.D. Thangadurai, *Applied Surface Science*, 556 (2021) 149814.
35. W. Liu, J. Zhang, C. Li, L. Tang, Z. Zhang and M. Yang, *Talanta*, 104 (2013) 204.
36. L. Zhang, M. Yin, J. Qiu, T. Qiu, Y. Chen, S. Qi, X. Wei, X. Tian and D. Xu, *Biosensors and Bioelectronics: X*, 10 (2022) 100102.
37. S. Meenakshi, S. Jancy Sophia and K. Pandian, *Materials Science and Engineering: C*, 90 (2018) 407.

38. M.F. Khanfar, N. Absi, E.S. Abu-Nameh, M.M. Saket, N. Khorma and R. Daoud, *International Journal of Electrochemical Science*, 14 (2019) 3265.
39. B. Bai, S. Jiang, L. Liu, X. Li and H. Wu, *Powder Technology*, 387 (2021) 22.
40. S.R. Obireddy and W.-F. Lai, *Pharmaceutics*, 13 (2021) 313.
41. T.-H. Zhao, Z.-Y. He and Y.-M. Chu, *Computational Methods and Function Theory*, 21 (2021) 413.
42. S.A. Iqbal, M.G. Hafez, Y.-M. Chu and C. Park, *Journal of Applied Analysis & Computation*, 12 (2022) 770.
43. H. Maleh, M. Alizadeh, F. Karimi, M. Baghayeri, L. Fu, J. Rouhi, C. Karaman, O. Karaman and R. Boukherroub, *Chemosphere*, (2021) 132928.
44. J. Pei, H. Zhao, F. Yang and D. Yan, *Langmuir*, 37 (2021) 6032.
45. S.K. Abdel-Aal, A. Ionov, R. Mozhchil and A.H. Naqvi, *Applied Physics A*, 124 (2018) 1.
46. Z. Dai, K. Wang, L. Li and T. Zhang, *International Journal of Electrochemical Science*, 8 (2013) 9384.
47. A. J. Hassani, Z. A. Mohd Ishak, A. R. Mohamed, *eXPRESS Polymer Letters*, 8 (2014) 177.
48. A.R. Kagdi, R.C. Pullar, S.S. Meena, F.E. Carvalho, C.S. Sandhu, R.B. Jotania, C. Prajapat and C. Basak, *Materials Chemistry and Physics*, 282 (2022) 125914.
49. M. Rostami, H. Mazaheri, A. H. Joshaghani, A. Shokri, *International Journal of Engineering*, 32 (2019) 1074.
50. H. Karimi-Maleh, R. Darabi, M. Shabani-Nooshabadi, M. Baghayeri, F. Karimi, J. Rouhi, M. Alizadeh, O. Karaman, Y. Vasseghian and C. Karaman, *Food and Chemical Toxicology*, 162 (2022) 112907.
51. J. Huang, X. Shen, R. Wang, Q. Zeng and L. Wang, *Rsc Advances*, 7 (2017) 535.
52. M.-K. Wang, M.-Y. Hong, Y.-F. Xu, Z.-H. Shen and Y.-M. Chu, *Journal of Mathematical Inequalities*, 14 (2020) 1.
53. J. Rouhi, S. Kakooei, S.M. Sadeghzadeh, O. Rouhi and R. Karimzadeh, *Journal of Solid State Electrochemistry*, 24 (2020) 1599.
54. J. Zoubir, N. Bougdour, C. Radaa, A. Idlahcen, I. Bakas and A. Assabbane, *Sensors International*, 3 (2022) 100160.
55. I. Saidi, I. Soutrel, F. Fourcade, A. Amrane, N. Bellakhal and F. Geneste, *Electrochimica Acta*, 191 (2016) 821.
56. R.A. Senthil, A. Selvi, P. Arunachalam, L.S. Amudha, J. Madhavan and A.M. Al-Mayouf, *Journal of Materials Science: Materials in Electronics*, 28 (2017) 10081.
57. C. Xin, L. Changhe, D. Wenfeng, C. Yun, M. Cong, X. Xuefeng, L. Bo, W. Dazhong, H.N. LI and Y. ZHANG, *Chinese Journal of Aeronautics*, (2021) 1.
58. H. Karimi-Maleh, C. Karaman, O. Karaman, F. Karimi, Y. Vasseghian, L. Fu, M. Baghayeri, J. Rouhi, P. Senthil Kumar and P.-L. Show, *Journal of Nanostructure in Chemistry*, (2022) 1.
59. F. Ebrahimi-Tazangi, J. Seyed-Yazdi and S.H. Hekmatara, *Journal of Alloys and Compounds*, 900 (2022) 163340.
60. R. Savari, J. Rouhi, O. Fakhar, S. Kakooei, D. Pourzadeh, O. Jahanbakhsh and S. Shojaei, *Ceramics International*, 47 (2021) 31927.
61. R. Savari, H. Savaloni, S. Abbasi and F. Placido, *Sensors and Actuators B: Chemical*, 266 (2018) 620.
62. A. H. Joshaghani, F. Soleimani, M. S. Fard, A. Shokri, *Journal of Nanoanalysis*, (2022) doi: 10.22034/jna.2022.1935754.1266.
63. Z. Savari, S. Soltanian, A. Noorbakhsh, A. Salimi, M. Najafi and P. Servati, *Sensors and Actuators B: Chemical*, 176 (2013) 335.
64. K. Karthikeyan, P. Karthikeyan, H.M. Baskonus, K. Venkatachalam and Y.M. Chu, *Mathematical Methods in the Applied Sciences*, (2021) 1.

65. F. Chahshouri, H. Savaloni, E. Khani and R. Savari, *Journal of Micromechanics and Microengineering*, 30 (2020) 075001.
66. T.-H. Zhao, M.-K. Wang, G.-J. Hai and Y.-M. Chu, *Revista de la Real Academia de Ciencias Exactas, Físicas y Naturales. Serie A. Matemáticas*, 116 (2022) 1.
67. Y. Nikodimos and M. Amare, *Journal of Analytical Methods in Chemistry*, 2016 (2016) 3612943.
68. M. Feizbahr, S. M. Mirhosseini, A. H. Joshaghani, *Express Nano Letters*, 1 (2020) 1.
69. S. Rashid, S. Sultana, Y. Karaca, A. Khalid and Y.-M. Chu, *Fractals*, 30 (2022) 2240026.
70. N. Naderi, M. Hashim, J. Rouhi and H. Mahmodi, *Materials science in semiconductor processing*, 16 (2013) 542.
71. F. Azimov, J. Kim, S.M. Choi and H.M. Jung, *Nanomaterials*, 11 (2021) 1557.
72. H. Savaloni, E. Khani, R. Savari, F. Chahshouri and F. Placido, *Applied Physics A*, 127 (2021) 1.
73. M. Nazeer, F. Hussain, M.I. Khan, E.R. El-Zahar, Y.-M. Chu and M. Malik, *Applied Mathematics and Computation*, 420 (2022) 126868.
74. G. Bharath, E. Alhseinat, R. Madhu, S.M. Mugo, S. Alwasel and A.H. Harrath, *Journal of Alloys and Compounds*, 750 (2018) 819.
75. Y.-M. Chu, B. Shankaralingappa, B. Gireesha, F. Alzahrani, M.I. Khan and S.U. Khan, *Applied Mathematics and Computation*, 419 (2022) 126883.
76. H. Karimi-Maleh, H. Beitollahi, P.S. Kumar, S. Tajik, P.M. Jahani, F. Karimi, C. Karaman, Y. Vasseghian, M. Baghayeri and J. Rouhi, *Food and Chemical Toxicology*, (2022) 112961.